Icarus 275 (2016) 97–106

Contents lists available at ScienceDirect

Icarus

journal homepage: www.elsevier.com/locate/icarus

Inversions of subsurface temperature and thermal diffusivity on the Moon based on high frequency of Chang'E-1 microwave radiometer data

Guangfei Wei[a], Xiongyao Li[a,*], Shijie Wang[b]

[a] Center for Lunar and Planetary Sciences, Institute of Geochemistry, Chinese Academy of Sciences, Guiyang 550081, China
[b] State Key Laboratory of Environmental Geochemistry, Institute of Geochemistry, Chinese Academy of Sciences, Guiyang 550081, China

ARTICLE INFO

Article history:
Received 6 July 2015
Revised 25 February 2016
Accepted 11 April 2016
Available online 19 April 2016

Keywords:
Moon
Subsurface
Regolith
Microwave

ABSTRACT

Thermal behavior of regolith reflects its thermophysical properties directly on the Moon. In this study, we employed the Fourier temperature model and inverted mean subsurface temperature and thermal diffusivity from high frequency of Chang'E-1 microwave radiometer data. The result showed that the mafic lunar mare endured higher thermal regime than that of feldspathic highland in a lunar cycle. As expected, the highland diffusivity with mean value 2.5 $\times$ 10^{-4} cm^2/s is greater than the mean value 0.3 $\times$ 10^{-4} cm^2/s of lunar mare. It indicated that the highland material responded more quickly than that of lunar mare to the changes of surface temperature in a diurnal day. In addition, thermal anomalous regions and hot/cold spots were also identified by diffusivity. For the thermal anomalous regions, Mare Tranquillitatis for example, with more contents of ($FeO+TiO_2$), agglutinate and high maturity index corresponded to greater diffusivity ($\sim$1.0 $\times$ 10^{-4} cm^2/s) and is more sensitive to the variations of temperature than the neighboring Mare Serenitatis ($\sim$0.3 $\times$ 10^{-4} cm^2/s). Thus, inversion and comparison of regolith thermophysical properties can reveal more information of geological evolution on the Moon.

1. Introduction

Thermal behavior of the Moon's near-surface reflects directly the nature of regolith. Due to the tenuous atmosphere of the Moon, the intensity of regolith radiation responses immediately to the changes of surface temperature. The temperature in the form of heat wave propagates downward along thermal gradient which is controlled by regolith thermophysical properties. To characterize this time- and depth-dependent thermal process, one-dimensional thermal model is widely used in the simulation on the basis of physical parameters that are measured from returned Apollo samples (Bauch et al., 2014; Fang and Fa, 2014; Vasavada et al., 1999; 2012). However, the parameters, thermal conductivity (κ) which is a function of both depth and temperature, and specific heat (C) which is a function of temperature (Keihm, 1984; Vasavada et al., 2012), are not fully constrained in most lunar areas besides the sampling sites.

Recently, Diviner Lunar Radiometer Experiment (DLRE) onboard Lunar Reconnaissance Orbiter has measured thermal radiation of the Moon globally. The unprecedented high spatial resolution data are used to infer near-surface thermophysical properties at lunar equator, thermal behaviors at cold traps of lunar south pole and even rock abundance (Bandfield et al., 2011; Paige et al., 2010; Vasavada et al., 2012). These large quantity of thermal observations provide good constrains on thermal emission and thermophysical properties of regolith, but are limited to the very near-surface of the Moon due to the shallow penetration depth (Vasavada et al., 2012).

In contrast, the regolith becomes more transparent for greater microwave wavelengths. Therefore, the observed microwave emission is correlated with the subsurface temperature and regolith thermophysical properties (Keihm and Langseth, 1975). As a result, it can at best characterize regolith thermophysical properties from surface to a depth of a few meters. Thus, it is necessary to establish a theoretical model to connect microwave observations to interpret the intensity and time-varying radio emission from the Moon. It can help us to better understand the global subsurface thermal regime, regolith thermophysical properties and even extend our knowledge about internal heat flow and geological evolution.

China has launched Chang'E-1 (CE-1) on October 24, 2007 successfully. During more than one year of orbiting at an altitude

* Corresponding author. Tel.: +86 189 850 29760; fax: +86 851 5893400.
E-mail address: lixiongyao@vip.skleg.cn (X. Li).

http://dx.doi.org/10.1016/j.icarus.2016.04.014
0019-1035/

about 200 km, large volume of brightness temperature (TB) data at 3.0, 7.8, 19.35, and 37 GHz are obtained by microwave radiometer (MRM) onboard the satellite. More details of CE-1's MRM and data processing are described in the work of Zheng et al. (2012). Based on CE-1 MRM data, Chan et al. (2010) and Zheng et al. (2012) find a strong anti-correlation between daytime and nighttime TB deviations at lunar mare. In addition, they also identify some cold spots that are located at young impact craters during noontime (Chan et al., 2010; Zheng et al., 2012). These thermal anomalies are of great interest and significance, which may be attributed to regolith compositions and rock abundance (Bandfield et al., 2011).

In order to investigate the subsurface temperature and thermophysical properties of regolith systematically, in this study, we employed the Fourier series which is a function of time, depth and thermal diffusivity to simulate variations of near-surface temperature. Additionally, all the TB data covering lunar surface are obtained near noontime or midnight (lunar local time) during the CE-1's life span. Hence, we selected the nighttime data to invert subsurface temperature and diffusivity for the purpose of reducing shadowing effect. Then we try to discuss the subsurface thermal state and regolith thermophysical properties beyond the only Apollo 15 and 17 in situ measurements.

In Section 2, we first introduce a Fourier series that is a function of time, depth and diffusivity as our temperature model. Then, inversion approach is introduced by building an inhomogeneous multi layer microwave radiative transfer model. In Section 3, as an example for our inversion results, mean subsurface temperature and thermal diffusivity are presented, and the anomalous thermal behaviors of lunar mare and impact craters are also identified. Then, the inversion results are validated by comparing with Apollo 15 and 17 in situ heat flow measurements. Thermal behaviors at lunar Mare Tranquillitatis and Serenitatis are compared and discussed as an example in Section 4, and further applications of our inversion results are also presented.

2. Inversion methodology

2.1. Temperature model

As noted above, the one-dimensional thermal model is a general method to simulate temperature variations on the Moon. However, the temperature- and depth-dependent thermophysical parameters (κ and C) are not widely determined when studying the global thermal behaviors, especially in the farside of the Moon. As the solar irradiance received by lunar surface shows a sine-like undulation, the subsurface temperature of a few centimeters regolith layers varies periodically. Here we employed a nearly forgotten method to describe lunar regolith temperature variation. Mathematically, the temperature as a function of depth (z), time (t) in the periodic state can be simulated by Fourier series as follows (Mezger and Strassl, 1959; Wesselink, 1948).

$$T(z,t) = T_0 + \sum_{n=1}^{\infty} T_n \exp(-\beta_n z)\cos(n\omega t - \beta_n z) \quad (1)$$

where $\beta_n = \sqrt{n\pi/(\alpha P)}$, is phase lag of surface temperature propagating inward against the original surface temperature. P is diurnal period of the Moon (29.53 earth days), α is thermal diffusivity that is determined by $\alpha = \kappa/(\rho C)$ and, ω is angular frequency. Because of the pronounced amplitude attenuating and phase shift of higher heat waves, the inward temperature distribution will be dominated by the fundamental wave $n = 1$ exclusively (Mezger and Strassl, 1959). Thus, Eq. (1) can be rewritten as

$$T(z,t) = T_m + T_a \exp\left(-\sqrt{\frac{\pi}{\alpha P}}z\right)\cos\left(\omega t - \sqrt{\frac{\pi}{\alpha P}}z\right) \quad (2)$$

where T_m is mean subsurface temperature (i.e. the temperature tends to be constant at greater depths), T_a is temperature amplitude. Note that the time-, depth- and diffusivity-dependent Eq. (2) is also a solution to one-dimensional heat conduction equation, which is determined by bulk thermophysical properties of regolith, namely solar albedo, latitude, density, thermal conductivity and heat capacity (Vasavada et al., 1999).

Linear fits of attenuation models for diffusivity at Apollo 15 and 17 landing sites indicate that the effective bulk diffusivity would be constant at depths > 15 cm, regardless of the near-surface properties (Langseth et al., 1976). That is, the time-varying surface temperature in the form of heat wave attenuates with depth in a decay constant $\beta = \sqrt{\pi/(\alpha P)}$ for the homogeneous thermal properties of regolith below the depth of 15 cm (Carslaw and Jaeger, 1959; Langseth et al., 1976). Therefore, the inversion diffusivity at greater depths (> 15 cm) is assumed to be a steady state value in this study, and it reflects how quickly the lunar regolith reacts to the changes of temperature in a diurnal cycle.

2.2. CE-1 MRM data reduction

With nadir view of CE-1's MRM (i.e., the observation angle equals 0°), it covered the Moon with full lunar day and night and obtained eight sets of global TB data during its one and a half years of observation (Zheng et al., 2012). However, the observed local time mainly focused on noontime and midnight. In this study, we selected nighttime data set which are less affected by shadowing effect. Additionally, in order to eliminate instability of TB data such as caused by instrument error, we normalized the nighttime data to midnight following the method of Zheng et al. (2012). For any data point on the lunar surface, the normalized midnight TB data ($TB_{midnight(normalized)}$) can be derived as

$$TB_{midnight(normalized)} = TB_{h(measured)} \times TB_{midnight(model)}/TB_{h(model)} \quad (3)$$

where $TB_{h(measured)}$ is observed TB value at local time h, $TB_{h(model)}$ and $TB_{midnight(model)}$ indicate the model values at local time h and midnight, respectively. They can be obtain by a seventh degree polynomial fitting scheme

$$TB_{h(model)} = \sum_{i=0}^{7} B_i \times h^i \quad (4)$$

where B_i $(i = 0 \cdots 7)$ are fitting coefficients.

For the low spatial resolution of MRM (with 30 km for the high frequency channels), the normalized data were collected and averaged in 1° × 1° bins. It is worth to note that the data sets are limited to 60°S–60°N because of (1) masking effect of brightness temperature caused by topographic shadows; (2) varies of local time with increasing latitude (Fang and Fa, 2014); and (3) the effect of topographic relief on ($FeO+TiO_2$) content retrieved from Clementine Ultraviolet/Visible (UV/Vis) data (Lucey et al., 1998).

With the same coverage as reduced TB data, we also retrieved ($FeO+TiO_2$) content limited to the range 60°S–60°N following the algorithms of Gillis et al. (2003, 2004) based on Clementine UV/Vis data. Thus, the average content of ($FeO+TiO_2$) corresponding to TB grids (with total of 360 × 120 bins) can be derived.

2.3. Inversion approach

To simulate the continuous temperature profile numerically, we divided regolith into multi-layers along the depth direction. Apollo 15 and 17 in situ heat flow measurements show that the temperature varies significantly in shallow depth (< 20 cm) during a lunar cycle (Langseth et al., 1976). Accordingly, we apply an exponential stratified method to give more discrete layers in upper 20 cm regolith. Measurement of returned lunar samples indicates that the

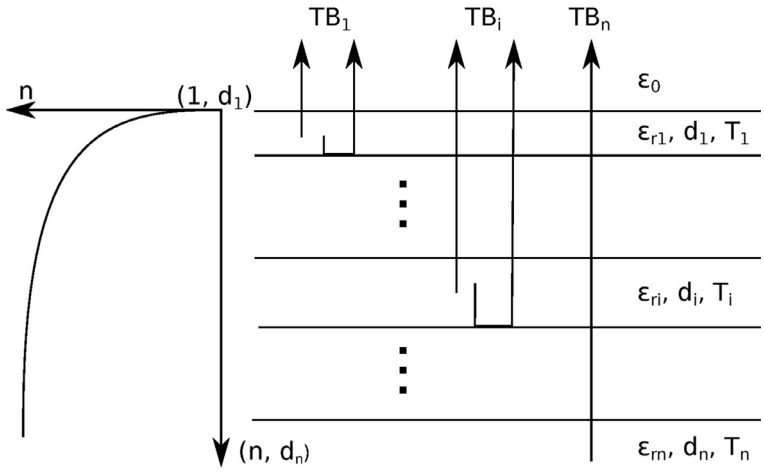

Fig. 1. Schematic of regolith division (left) and inhomogeneous multi-layer of microwave radiative transfer model (right). n is the number of regolith layers. ε_0 is relative dielectric constant of free space. ε_{ri}, d_i and T_i are relative dielectric constant, thickness and temperature of the ith ($i = 1, \ldots, n$) layer, respectively.

bulk density of regolith (ρ) is related to buried depth (z, in meters), and it can be expressed as (Heiken et al., 1991)

$$\rho(z) = 1.919\frac{z+0.122}{z+0.18} \tag{5}$$

To establish the multi-layers model, we rewrite Eq. (5) as

$$z(\rho) = -0.18\frac{\rho-1.3}{\rho-1.92} \tag{6}$$

Thus, the depth in Eq. (6) becomes a function of bulk density. Considering the density variation from surface 1.3 g/cm^3 to the maximum 1.9 g/cm^3 of the bottom, the regolith can be divided into 61 layers (the last layer is assumed to be bed rock) for the density intervals of 0.01 g/cm^3. The thickness of regolith layer d_i ($i = 1, \ldots, n, n = 62$), therefore, increases exponentially from the top layer to the bottom one (as shown in Fig. 1, left panel). As a result, the time-varying temperature of each layer (T_i) can be simulated based on Eq. (2).

In order to calculate microwave emission contributed from all the layers, we employed a microwave radiative transfer theory in this study. The fluctuation dissipation theory has been widely used to simulate brightness temperature and invert the thickness of lunar regolith (e.g., Fa and Jin, 2007a, b; Jin and Fa, 2009; Zhou et al., 2010; Gong and Jin, 2012). Here, we apply this theory on the inhomogeneous multi-layer model (see Fig. 1, right panel).

For the nadir viewing of CE-1's MRM, the contribution of brightness temperature (TB_i) from ith layer can be wrote as (Jin, 1984; Zhou et al., 2010)

$$\begin{aligned} TB_i = {} & \left(1-e^{-2k_i''d_i}\right)\left(1+\left|R_{i(i+1)}\right|^2 e^{-2k_i''d_i}\right)\prod_{j=0}^{i-1} \\ & \times\left[\left(1-\left|R_{i(i+1)}\right|^2\right)e^{-2k_j''d_j}\right]T_i \end{aligned} \tag{7}$$

For the bottom layer the contribution of brightness temperature (TB_n) can be expressed as (Jin, 1984; Zhou et al., 2010)

$$TB_n = \prod_{j=0}^{n}\left[\left(1-\left|R_{j(j+1)}\right|^2\right)e^{-2k_j''d_j}\right]T_n \tag{8}$$

Combining Eqs. (7) and (8), the total contribution of brightness temperatures from the multi-layer can be summed up as follows (Jin, 1984; Zhou et al., 2010)

$$\begin{aligned} TB = {} & k_0\sum_{i=1}^{n-1}\frac{\varepsilon_{ri}''}{2k_{iz}''}\left[1-e^{-2k_{iz}''d_i}\right] \\ & \cdot\left[1+\left|R_{i(i+1)}\right|^2 e^{-2k_{iz}''d_i}\right]\prod_{j=0}^{i-1}\left[\left|X_{j(j+1)}\right|^2 e^{-2k_{iz}''d_i}\right]T_i \\ & + \frac{k_0\varepsilon_{rn}''}{2k_{nz}''}\left|X_{j(j+1)}\right|^2 e^{-2k_{jz}''d_j}\prod_{j=0}^{n-1}\left[\left|X_{j(j+1)}\right|^2 e^{-2k_{iz}''d_i}\right]T_n \end{aligned} \tag{9}$$

where n is layer number, ε_{ri} ($i = 1, \ldots, n$) is relative dielectric constant, k_0 is wave number of free space, k_{iz} is wave number along z direction of layer i, and k_{iz}'' is imaginary part of k_{iz}. $R_{i(i+1)}$ and $X_{i(i+1)}$ are reflection coefficient and transmission coefficient between ith and $(i+1)$th layers, respectively.

Laboratory measurement of relative dielectric constant ($\varepsilon_r = \varepsilon' + i\varepsilon''$) from Apollo samples shows that ε_r is depended upon regolith bulk density and ($FeO+TiO_2$) content, S (Heiken et al., 1991).

$$\varepsilon' = 1.92^{\rho} \tag{10a}$$

$$\tan\delta = 10^{0.038S+0.312\rho-3.26} \tag{10b}$$

where $\tan\delta = \varepsilon''/\varepsilon'$ is loss tangent. ε' and ε'' are real and imaginary parts of dielectric constant, respectively.

Therefore, the dielectric constant of each layer (as shown in Fig. 1, ε_{ri}) can be calculated based on Eqs. (5) and (10). Consequently, the theoretical TB that is depended on thermophysical properties of regolith can be simulated by combining Eqs. (2), (5), (9) and (10).

In order to avoid an ill-posed inversion problem, we used the least square method to find the most appropriate values T_m, T_a and α by minimizing the differences of TB between theoretical calculations and observations. In this study, we inverted these parameters by using high frequency of TB data. It can be defined as

$$T_m, T_a, \alpha = \arg\min\left[\left(TB_{37}-TB_{37}^{o}\right)^2 + \left(TB_{19}-TB_{19}^{o}\right)^2\right] \tag{11}$$

where, TB_{37} and TB_{19} are calculated brightness temperatures at 37 and 19.35 GHz, respectively. The superscript "o" denotes observed values.

It is essential to set initial values for mean subsurface temperature, temperature amplitude and thermal diffusivity $x_0 =$

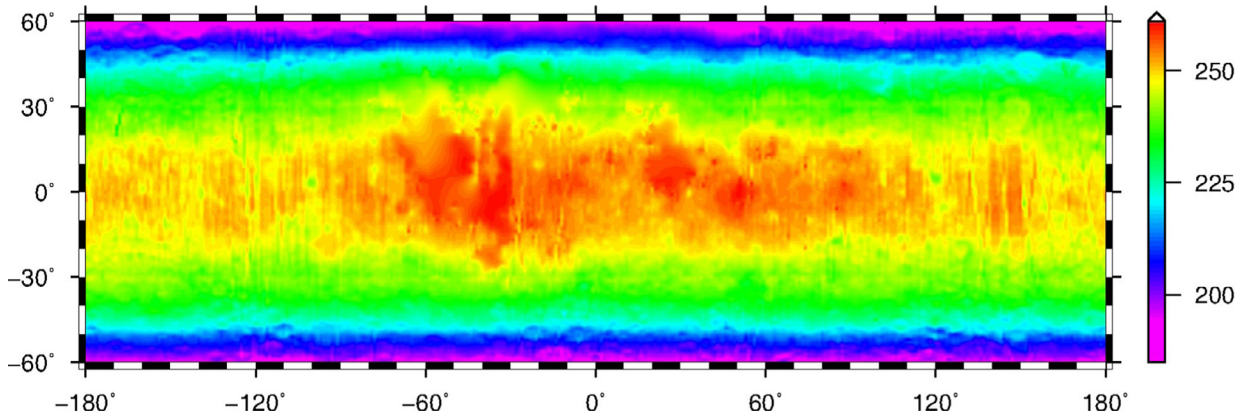

Fig. 2. Inverted mean subsurface temperature from normalized nighttime 37 and 19.35 GHz data.

$(T_{m0}, T_{a0}, \alpha_0)$ before searching the optimal values. These prior information were given based on Apollo 15, 17 in situ measurements. The mean subsurface temperature at a depth of 1 m was detected approximately 251 K at Apollo 15 landing site (Langseth et al., 1972). The daily amplitude of surface temperature was also measured for −150 K at Apollo 17 landing site (Keihm and Langseth, 1973). Additionally, revised long-term heat flow values indicate an average diffusivity 0.8×10^{-4} cm^2/s at Apollo 15, 17 landing sites (Langseth et al., 1976). Therefore, the initial values were given as $x_0 = (251, -150, 0.8 \times 10^{-4})$.

3. Results

3.1. Mean subsurface temperature

As indicated by Apollo 17 heat flow experiment, there is a ubiquitous 2 cm thick porous dust layer with extreme low thermal conductivity (in the order of 10^{-5} W/(m K)) overlying more compacted regolith layer (Keihm and Langseth, 1973). This high insulated layer inhibits surface heat wave into subsurface and causes drastically decrease of temperature. At greater depths (> 10 cm), the conductivity gradient of regolith increases with depth substantially (Keihm and Langseth, 1973). Since the temperature attenuates with depth, the variation of subsurface temperature becomes nearly undetectable at depth of ~50 cm as detected by Apollo 15 in situ experiment (Langseth et al., 1972). Fig. 2 shows the mean subsurface temperature which indicates a thermal equilibrium state at greater depths.

Apparently, the temperature of lunar mare is relative higher than that of highland. That is, mare materials stores more thermal energy by conducting heat flux into and out of subsurface. In addition, to characterize and compare the global thermal regime varying with latitude, we employed an cosine function to fit the subsurface temperature as follows (Fang and Fa, 2014).

$$\langle T_{\mathrm{sub}}(\phi)\rangle = T_{\mathrm{sub0}} \cos^b \phi \tag{12}$$

where T_{sub0} is the mean subsurface temperature at lunar equator, ϕ is the latitude, and b is exponent. For determining T_{sub0} and b, we processed the inverted subsurface temperature data in the following steps. (1) Calculating the average temperature of each latitude band along longitude, i.e., 1° × 360°. (2) Using least-square method to fit the mean temperature that is a function of latitude. Fig. 3 shows the inverted mean subsurface temperature and best-fitting curves related to latitude.

As indicated by the fitting curve (red line, $253\cos^{0.38}\phi$), the subsurface temperature with greater fitting exponent decreases quickly toward higher latitude than previous work (blue line, $255\cos^{0.36}\phi$). The fluctuation of inverted subsurface temperature (black line) might be caused by topographic relief (especial for cratered highland), rock abundance and variation of ($FeO+TiO_2$) content.

3.2. Map of thermal diffusivity

As shown in Fig. 4, at first glance it is apparent that thermal diffusivity of highland with an average value of about 2.5×10^{-4} cm^2/s is much greater than lunar mare with an mean value 0.3×10^{-4} cm^2/s. With greater diffusivity, material of highland reacts to the changes of surface temperature quickly in a diurnal day. Additionally, the hot/cold spots identified by Price et al. (2003), Zheng et al. (2012) also correspond to greater thermal diffusivity as labeled by A–E in Fig. 4. This may be mainly attributed to rock fragment covering the ejecta blankets comparing to the surrounding grained regolith (Bandfield et al., 2011).

Nevertheless, some areas including Mare Tranquillitatis and South of Oceanus Procellarum present greater diffusivity (with average values of 1–1.5 × 10^{-4} cm^2/s) than surrounding maria areas. This may explain why there are strong anti-correlation of day/night brightness temperature deviations which have been reported by Chan et al. (2010) and Zheng et al. (2012). That is, these areas react to changes of surface temperature more quickly in a lunar diurnal day. Geologically, the relative uniform distribution of diffusivity in lunar mare indicates the homogeneous evolution of regolith. However, for the inhomogeneous highland, the evolution of regolith thermal properties may related to the Moon's surface geological evolution such as impact gardening.

3.3. Inversion validation and uncertainty

In this section, we have validated our inversion results by comparing with Apollo 15 and 17 in situ measurements and stated the inversion uncertainty. Strictly speaking, it is not very appropriate for this kind of validation because of the different spatial coverage. Nevertheless, it can also provide reasonable reference values for our inversion results.

In order to make a best superposition for the center of field of view on Apollo 15 and 17 landing sites, the CE-1 TB data covering the landing sites that are limited in ±0.1° are selected, respectively. Fig. 5 (black lines) shows the inverted instantaneous temperature profiles without internal heat flow effects at the landing areas. It shows that the subsurface temperature is free from surface temperature disturbance and becomes constant below the depth of ~30 cm. Considering the internal heat flow effect (here we applied the same thermal gradients for 2.52 and 1.35 K/m as Apollo 15 (probe 2) and 17 (probe 1) detections for convenient comparisons), the modified subsurface temperatures

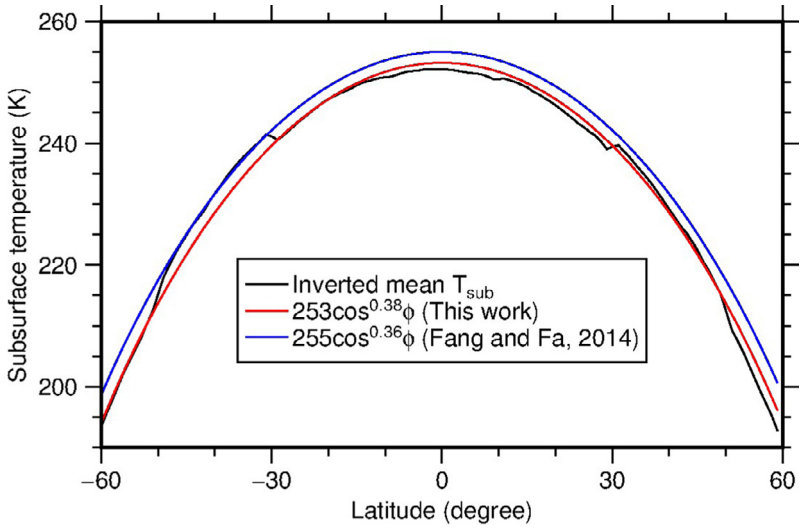

Fig. 3. Shown is inverted mean subsurface temperature and comparison of its best-fitting curve derived from Eq. (12). The black solid line is the inverted mean subsurface temperature, which corresponds to the best-fitting curve marked by red line. The blue line indicates the best-fitting curve of mean subsurface temperature inverted from Chang'E-2 brightness temperature in the work of Fang and Fa (2014). (For interpretation of the references to color in this figure legend and text, the reader is referred to the web version of this article.)

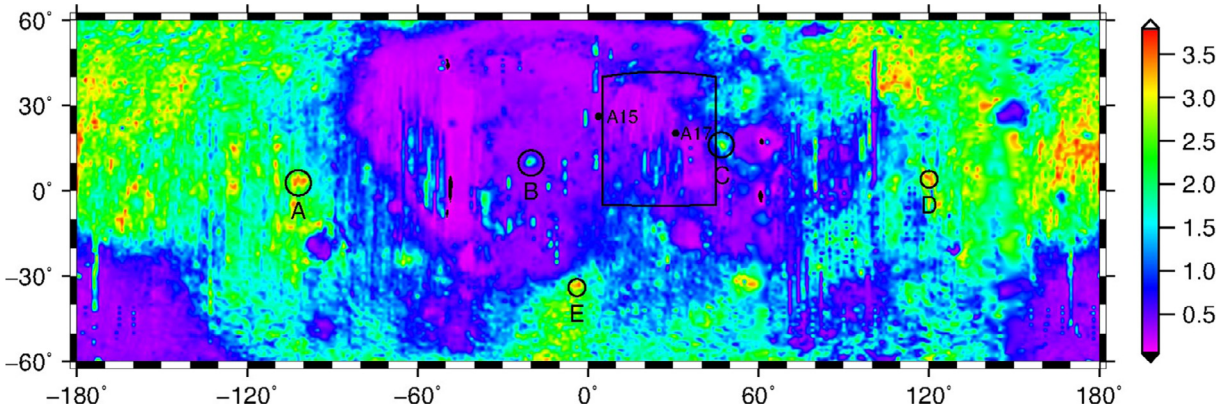

Fig. 4. Shown is distribution of thermal diffusivity ($\times$ 10^{-4} cm^2/s) inverted from 19.35 and 37 GHz of CE-1 microwave radiometer data. Enclosed areas labeled by A–E correspond to craters of Lents, Copernicus, Proclus, King and Hell-Q. The points labeled by A15 and A17 denote the Apollo 15 and 17 landing sites, respectively. The area enclosed by box is our study area including Mare Serenitatis and Mare Tranquillitatis.

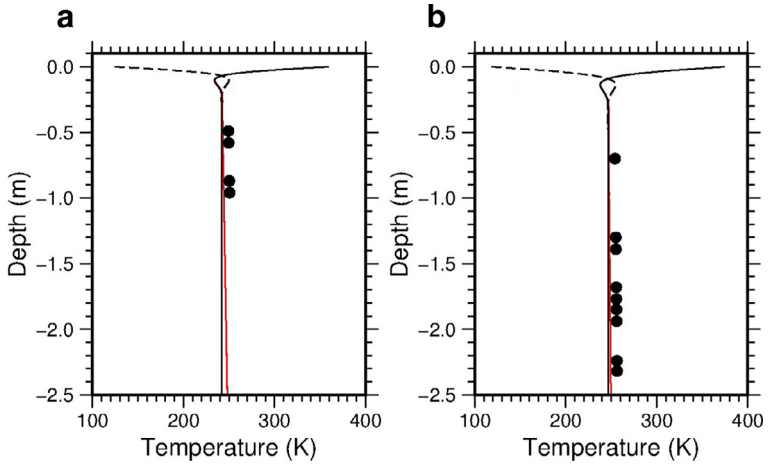

Fig. 5. Inverted instantaneous temperature profiles with (red lines) and without (black lines) internal heat flow effects at Apollo 15 (a) and 17 (b) landing sites. The solid and dashed black lines indicate the maximum and minimum temperatures in a lunar day, respectively. The thermal gradients are given 2.52 and 1.35 K/m that are derived from Apollo 15 (probe 2) and 17 (probe 1) measurements (Langseth et al., 1976). The dots in (a) and (b) denote the mean subsurface temperatures detected from Apollo 15 (probe 2) and 17 (probe 1) in situ heat flow measurements, respectively (Langseth et al., 1976). (For interpretation of the references to color in this figure legend and text, the reader is referred to the web version of this article.)

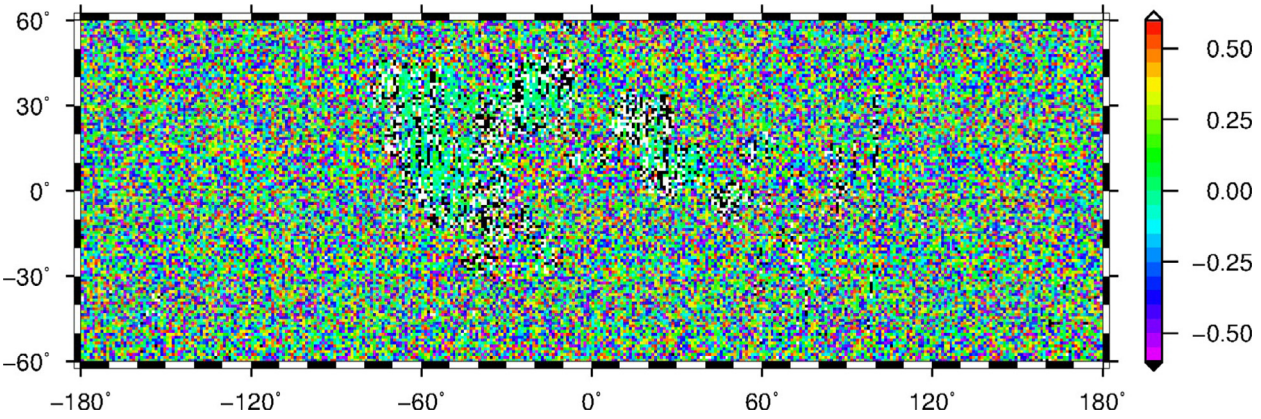

Fig. 6. Shown is difference of inverted mean subsurface temperature (K) between sounding data and MRM data with random noise disturbance. The noise is uniformly distributed within $[-0.5, 0.5]$ K.

(red lines) are 5–7 K lower than the Apollo measurements (dots) (Langseth et al., 1976). However, it is worth noting that the mean subsurface temperature detected by Apollo 15 probe 1 is 2 K greater than that of probe 2, whereas they are spaced only about 10 m apart (Langseth et al., 1976). For the large spatial coverage of CE-1's MRM (30 km scale), the differences of subsurface temperature between our inversion results and Apollo 15 and 17 in situ measurements may be attributed to the variations of internal heat flows and/or thermophysical properties of regolith. Detection of heat flow in large scale of future lunar exploration may improve the accuracy of temperature profiles.

Thermal diffusivity of returned Apollo 11, 12, 14, 15, 16, 17 samples has been measured in terrestrial laboratory by directed or indirected (calculated from the relation $\alpha = \kappa/(\rho C)$) methods, which shows that it largely depends on temperature, atmosphere pressure and mineral composition (e.g. Horai et al., 1970; Cremers, 1973; Cremers and Hsia, 1973; 1974; Cremers, 1975; Horai and Winkler, 1976). For example, measurement of Apollo 11 samples shows that thermal diffusivity of breccias is lower and less dependent on temperature than those of crystalline igneous rocks over the temperature range 150–440 K (Horai and Winkler, 1980). Therefore, it is necessary to obtain diffusivity by in situ measurement for better understand the nature of regolith.

The best fitting for transient temperature data at Apollo 15 landing site indicates that the diffusivity increases from 0.18×10^{-4} cm^2/s to 0.71×10^{-4} cm^2/s as a function of depth (0–96 cm) (Langseth et al., 1976). Which validates our inversion result $\sim 0.24 \times 10^{-4}$ cm^2/s at the corresponding site (see A15 of Fig. 4). The inverted diffusivity at Apollo 17 landing area (see A17 of Fig. 4) is $\sim 0.42 \times 10^{-4}$ cm^2/s that is 0.26×10^{-4} cm^2/s lower than the detected transient mean values. Since the Apollo 17 landing site locates in the transition region between Mare Tranquillitatis and Mare Serenitatis, the inverted diffusivity at 30 km scale reveals regional thermophysical properties of regolith rather than the pinpoint of Apollo 17. Nevertheless, the inversion result is also comparable to Apollo 17 derivations which are in the same order of magnitude.

Additionally, inversion results might become uncertainty if observations are disturbed by noises. Therefore, it is necessary to state inversion errors caused by noises. Here, we assume that a random noise uniformly distributed within $[-0.5, 0.5]$ K was added to MRM data. Based on these artificial data, mean subsurface temperature and thermal diffusivity were inverted.

Fig. 6 shows difference of inverted subsurface temperature (ΔT_{sub}) between sounding data and MRM data with noise disturbance. Expectantly, ΔT_{sub} distributes randomly on the Moon. Nevertheless, values of lunar mare vary drastically than that of highland. This may be caused by high content of $(FeO + TiO_2)$ at maria regions. Note that values of ΔT_{sub} within $[-0.6, 0.6]$ K accounted for 95% of total number of points. That is, the inverted mean subsurface temperature is relatively stable, and inversion error caused by noise within $[-0.5, 0.5]$ K can be neglected.

As shown in Fig. 7, diffusivity difference ($\Delta\alpha$) of highland tends to be 0, while $\Delta\alpha$ of lunar mare varies mainly within $[-0.2, 0.2] \times 10^{-4}$cm^2/s. It shows that the effect of noise on diffusivity of highland can be neglected. However, the diffusivity of lunar mare is sensitive to $(FeO + TiO_2)$ content which plays a part in microwave emission. It is worth noting that $\Delta\alpha$ within $[-0.2, 0.2] \times 10^{-4}$cm^2/s accounts for 94% of the total number of points, and inversion errors of lunar mare tend to be greater for larger noises.

4. Discussion and application

4.1. Discussion

As noted above, the very interested and significant thermal anomalies of mare regions (e.g., Mare Tranquillitatis) and impact craters (e.g., Copernicus and King) have been characterized by inverted diffusivities. It reveals special geological processes such as impact gardening and space weathering on the Moon. Considering the large spatial coverage of CE-1's MRM, here we selected a study area from lunar mare (enclosed by box in Fig. 4) for further discussion.

With advantage of great penetration depth for microwave, the brightness temperature reveals the total thermal emissions from all subsurface layers. Employing the temporal and spatial normalization method as described in Section 2.2, Fig. 8 shows the normalized brightness temperature of the study area at noontime and midnight. Obviously, the averaged TB of Mare Tranquillitatis at noontime (Fig. 8a) is ~290 K which is about 30 K higher than that of Mare Serenitatis. By contrast, it decreases significantly to ~220 K during midnight (Fig. 8b), which is lower than ~230 K of Mare Serenitatis. This thermal behaviors have also been characterized by infrared brightness temperature from DLRE. As shown in Fig. 9, it also shows an obvious anti-correlation of day/night thermal behaviors between the two maria areas.

To account for this thermal anomaly, Fig. 10 shows an enlarged view for the boxed area of Fig. 4. As expected, the mean diffusivity of Mare Tranquillitatis is $\sim 1.0 \times 10^{-4}$ cm^2/s which is greater than $\sim 0.3 \times 10^{-4}$ cm^2/s of Mare Serenitatis. That is, Mare Tranquillitatis absorbs solar radiation in daytime and emits to outer space during nighttime more quickly than Mare Serenitatis does. Thus, it results in different thermal behaviors for Mare Tranquillitatis and Mare Serenitatis as shown in Figs. 8 and 9.

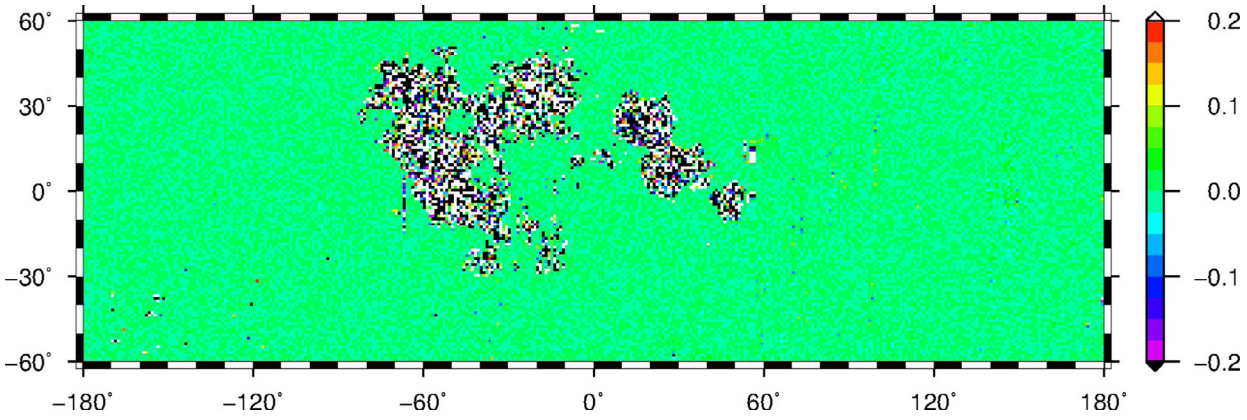

Fig. 7. Shown is difference of inverted thermal diffusivity ($\times 10^{-4}$cm^2/s) between sounding data and MRM data with random noise disturbance.

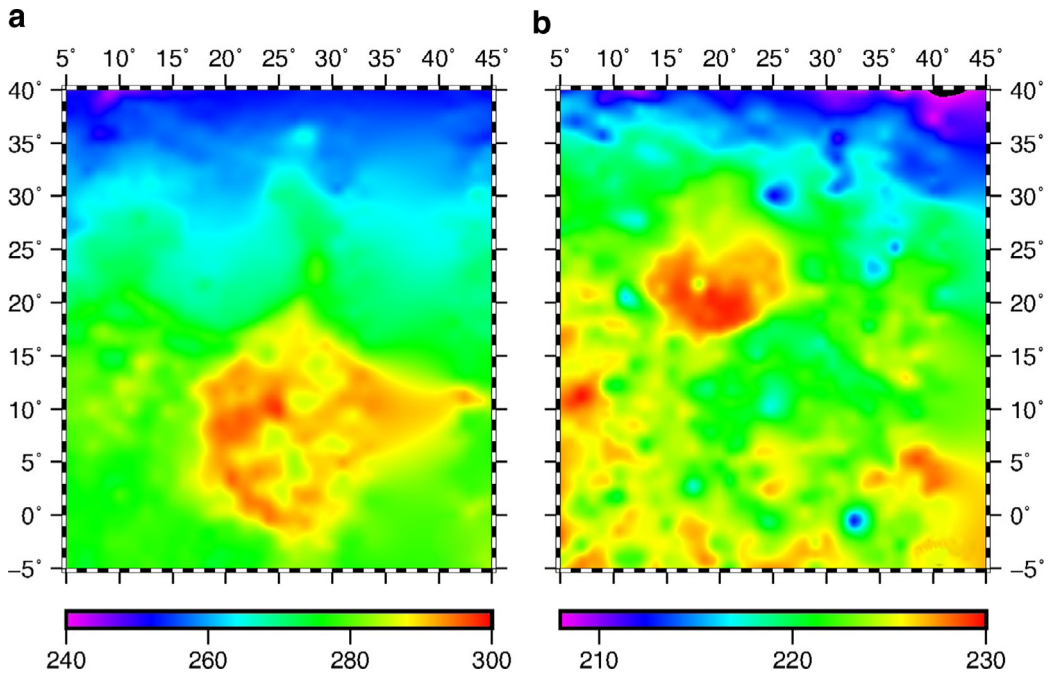

Fig. 8. Shown are normalized brightness temperature during noontime (a) and midnight (b) at the study area. Note that the region located in the north is Mare Serenitatis, and the neighboring region located in the south is Mare Tranquillitatis. This thermal behavior has also been characterized by Fig. 8 of Zheng et al. (2012).

The diffusivity difference between Mare Tranquillitatis and Mare Serenitatis may be attributed to their different thermophysical properties of the Moon's material. Fig. 11a and b shows that there are relative higher contents of ($FeO+TiO_2$) and agglutinate on Mare Tranquillitatis than that of Mare Serenitatis. This may differentiate the regolith thermal behaviors between the two maria areas by changing thermal conductivity and bulk capacity.

Additionally, the lunar surface has endured long-term impact gardening, meteorite bombardment, the effect of solar irradiation and etc. The so called space weathering history is also the process of soil maturation. As a result, the more mature the soil is characterized by a smaller mean particle size, larger contents of metallic iron and agglutinate (Shevchenko et al., 2003). Fig. 11c shows the distribution of maturity index derived from Clementine multispectral data as in the work of Pieters et al. (2006). Consistently, Mare Tranquillitatis with higher content of agglutinate is more mature than Mare Serenitatis. It indicates that higher maturation soils tends to be more sensitive to the surface temperature fluctuation. Thus, it can be inferred that the regolith thermal behavior is related to the process of the Moon's surface geological evolution. In the future of work, we would like to discuss the effects of degrees of soil maturity, rock abundance on the Moon's surface thermal behavior, especially on fresh impact craters.

4.2. Application

In this work, we employed the Fourier function (Eq. (2)) as the Moon's regolith temperature model. As examples, we inverted mean subsurface temperature from high frequency of CE-1 brightness temperature data. Regolith thermal behavior is dominated by thermophysical properties, which has been discussed in the form of thermal diffusivity. Since the thermal conductivity and specific heat are key parameters to study lunar regolith thermal emission and thermophysical properties, it is a kind of way to apply the subsurface temperature and diffusivity on exploration of regolith evolution. It also provides some constrains on regolith thermophysical properties and a possible way to study the interesting hot/cold spots on the Moon.

As measured by Apollo 15 and 17 heat flow experiments, the subsurface thermal regime is dominated by internal heat flow below a depth of 50 cm (Langseth et al., 1972). It plays a part in subsurface thermal state especial for permanently shadowed areas of

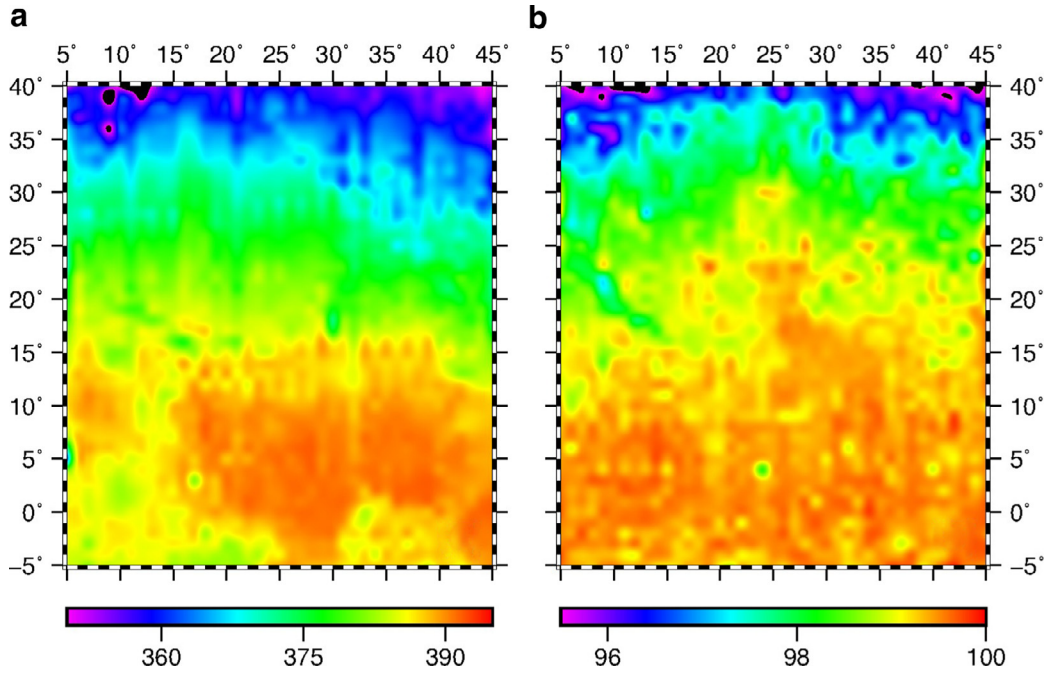

Fig. 9. Shown are infrared brightness temperature at noontime (a) and midnight (b) derived from channel 7 of DLRE data. Note that the data were also averaged by 1° × 1° bin for convenient comparison with CE-1 MRM data.

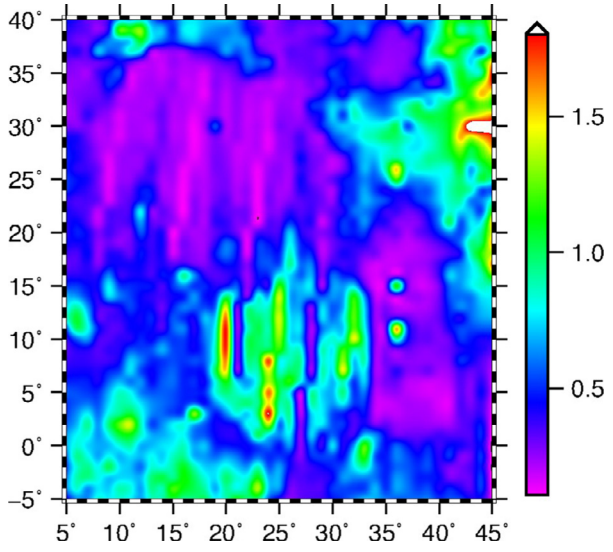

Fig. 10. Shown is thermal diffusivity (× 10^{-4} cm^2/s) of the study area that is enlarged from the boxed area of Fig. 4.

lunar south pole (Paige et al., 2010). Additionally, detection of heat flow also provides a clue to the evolution of radioactive elements. Based on the repeat coverage of CE-1 microwave brightness temperature data, it provides a possible way to retrieve internal heat flow for the great penetration depth of microwave wavelength. For example, the temperature model of Eq. (2) can be further rewritten as $T(z,t) = T_m + T_a \exp\left(-\sqrt{\pi/(\alpha P)}z\right)\cos\left(\omega t - \sqrt{\pi/(\alpha P)}z\right) + gz$, where g is geothermal gradient, i.e., $g = \partial T/\partial z$. It may be a new approach to retrieve internal heat flow (F) from the relation $F = \kappa \partial T/\partial z$. In the future work, we would like to retrieve global heat flow from low frequency (3 and 7.8 GHz) of CE-1 brightness temperature data.

5. Conclusions

Thermal behavior directly reflects the nature of lunar regolith. In this work, we employed Fourier function as temperature model to characterize thermophysical properties of lunar regolith especial for the thermal anomalous areas. Then we established an inhomogeneous multi layer microwave radiative transfer model and inverted mean subsurface temperature and thermal diffusivity from high frequency of CE-1 MRM data. Some interesting and significant results were derived as follows.

Several thermal anomalous areas located in lunar mare (e.g., Mare Tranquillitatis, South of Oceanus Procellarum) were identified and showed a strong anti-correlation between daytime and nighttime brightness temperatures, which indicated a special geological process such as impact gardening and space weathering. The diffusivity of highland with an average value 2.5 × 10^{-4} cm^2/s is greater than the mean value 0.3 × 10^{-4} cm^2/s of lunar mare. This accounts for the significant temperature variation at highland. In addition, we also identified some hot/cold spots with greater diffusivity covering young impact craters. These thermal anomalies may be related to abundant of rock fragments covering the fresh ejection.

For the large spatial coverage of CE-1's MRM, we selected a typical anomalous area Mare Tranquillitatis as an example for further discussion. The result showed that Mare Traquillitatis with greater diffusivity (~1.0 × 10^{-4} cm^2/s) corresponding to more contents of ($FeO+TiO_2$), agglutinate and high maturity index than the neighboring Mare Serenitatis (~0.3 × 10^{-4} cm^2/s). This may differentiate their thermal behaviors in a lunar cycle. On the other hand, observation of regolith thermal behavior and inversion of thermophysical parameters might provide a way to study the Moon's geological evolution.

Acknowledgments

This work was supported by the National Natural Science Foundation of China (General Program: Nos. 41373067, 41403057, 41572037; Major Program: No. 41490630) and

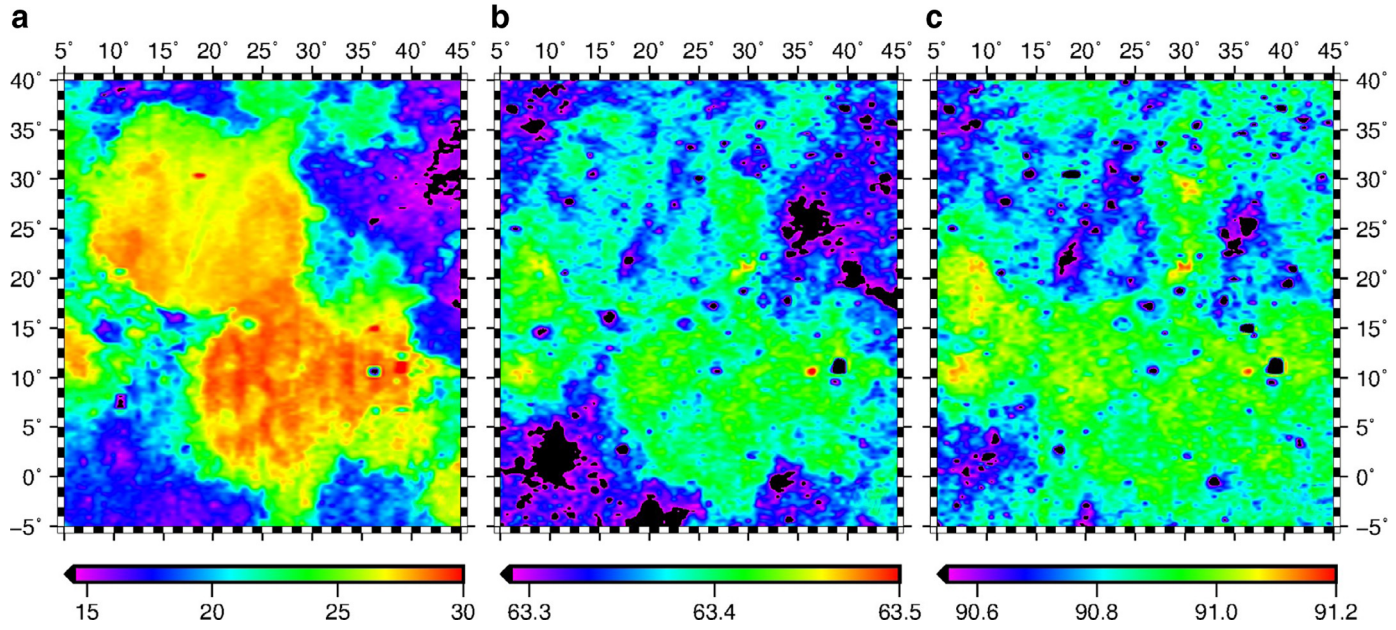

Fig. 11. Distribution of ($FeO+TiO_2$) (a), agglutinate (b) in percentage and maturity index (c) at the study area. The content of ($FeO+TiO_2$) was inverted from Clementine UVVIS data based on the algorithms of Gillis et al. (2003, 2004). Agglutinate content and maturity index were also derived from Clementine multi-spectral data as in the work of Pieters et al. (2006).

Youth Innovation Promotion Association of CAS (No. 2014359). Clementine UVVIS data were available at http://www.mapaplanet.org/explorer/moon.html. DLRE data were available at PDS Geosciences Node (http://pds-geosciences.wustl.edu/about/default.htm). CE-1 microwave radiometer data were provided by the National Astronomical Observatories, Chinese Academy of Sciences. Figures were created using the Generic Mapping Tool of Wessel and Smith (1991).

References

Bandfield, J.L., Ghent, R.R., Vasavada, A.R., et al., 2011. Lunar surface rock abundance and regolith fines temperatures derived from LRO Diviner Radiometer data. J. Geophys. Res. 116 (12), 1–18.

Bauch, K.E., Hiesinger, H., Helbert, J., et al., 2014. Estimation of lunar surface temperatures and thermophysical properties: Test of a thermal model in preparation of the MERTIS experiment onboard BepiColombo. Planet. Space Sci. 101, 27–36. doi:10.1016/j.pss.2014.06.004.

Carslaw, H.S., Jaeger, J.C., 1959. Conduction of Heat in Solids, second ed. Clarendon Press, Oxford.

Chan, K.L., Tsang, K.T., Kong, B., et al., 2010. Lunar regolith thermal behavior revealed by Chang'E-1 microwave brightness temperature data. Earth Planet. Sci. Lett. 295 (1–2), 287–291. doi:10.1016/j.epsl.2010.04.015.

Cremers, C.J., 1973. Thermophysical properties of Apollo 12 fines. Icarus 18 (2), 294–303. doi:10.1016/0019-1035(73)90212-1.

Cremers, C.J., 1975. Thermal properties of Apollo 14 fines. J. Geophys. Res. 80 (32), 4466–4470.

Cremers, C.J., Hsia, H.S., 1973. Thermal conductivity and diffusivity of Apollo 15 fines at low density. Proc. Fourth Lunar Science Conf. vol. 3, 2459–2464.

Cremers, C.J., Hsia, H.S., 1974. Thermal conductivity of Apollo 16 lunar fines. In: Proc. Fifth Lunar Science Conf., vol. 3, pp. 2703–2708.

Fa, W., Jin, Y.-Q., 2007a. Quantitative estimation of helium-3 spatial distribution in the lunar regolith layer. Icarus 190 (1), 15–23. doi:10.1016/j.icarus.2007.03.014.

Fa, W., Jin, Y.-Q., 2007b. Simulation of brightness temperature from lunar surface and inversion of regolith-layer thickness. J. Geophys. Res. 112 (E5), E05003. doi:10.1029/2006JE002751.

Fang, T., Fa, W., 2014. High frequency thermal emission from the lunar surface and near surfacetemperature of the Moon from Chang'E-2 microwave radiometer. Icarus 232, 34–53.

Gillis, J.J., Jolliff, B.L., Elphic, R.C., 2003. A revised algorithm for calculating TiO_2 from Clementine UVVIS data: A synthesis of rock, soil, and remotely sensed TiO_2 concentrations. J. Geophys. Res. 108 (E2), 5009.

Gillis, J.J., Jolliff, B.L., Korotev, R.L., 2004. Lunar surface geochemistry: Global concentrations of Th, K, and FeO as derived from lunar prospector and Clementine data. Geochim. Cosmochim. Acta 68 (18), 3791–3805.

Gong, X., Jin, Y.-q., 2012. Microwave brightness temperature of cratered lunar surface and inversions of the physical temperature profile and thickness of regolith layer. Radio Sci. 47 (RS1012), 1–11. doi:10.1029/2011RS004791.

Heiken, G.H., Vaniman, D.T., French, B.M., 1991. Lunar Sourcebook – A User's Guide to the Moon. Cambridge University Press, London.

Horai, K., Winkler, J.J.L., 1980. Thermal diffusivity of two Apollo 11 samples, 10020,44 and 10065,23: Effect of petrofabrics on the thermal conductivity of porous lunar rocks under vacuum. In: Proc. Lunar Planet. Sci. Conf. 11th, pp. 1777–1788.

Horai, K.-i., Simmons, G., Kanamori, H., et al., 1970. Thermal diffusivity and conductivity of lunar material. Science 167 (3918), 730–731.

Horai, K.-i., Winkler, J.L., 1976. Thermal diffusivity of four Apollo 17 rock samples. In: Proc. Lunar Sci. Conf. 7th, pp. 3183–3204.

Jin, Y.-Q., 1984. Wave approach to brightness temperature from a bounded layer of random discrete scatterers. Electromagnetics 4 (2–3), 323–341. doi:10.1080/02726348408908121.

Jin, Y.-Q., Fa, W., 2009. An inversion approach for lunar regolith layer thickness using optical albedo data and microwave emission simulation. Acta Astronaut. 65 (9–10), 1409–1423. doi:10.1016/j.actaastro.2009.03.082.

Keihm, S., Langseth, M., 1973. Surface brightness temperatures at the Apollo 17 heat flow site: Thermal conductivity of the upper 15 cm of regolith. In: Proc. Lunar Sci. Conf. 4th, vol. 4, pp. 2503–2513.

Keihm, S.J., 1984. Interpretation of the lunar microwave brightness temperature spectrum - Feasibility of orbital heat flow mapping. Icarus 589, 568–589. doi:10.1016/0019-1035(84)90165-9.

Keihm, S.J., Langseth, M.G., 1975. Microwave emission spectrum of the moon: Mean global heat flow and average depth of the regolith.. Science 187 (4171), 64–66. doi:10.1126/science.187.4171.64.

Langseth, G.M., Keihm, S.J., Peters, K., 1976. Revised lunar heat-flow values. In: Proc. Lunar Sci. Conf. 7th, pp. 3143–3171.

Langseth, M.G., Clark Jr., S.P., Chute Jr., J.L., et al., 1972. The Apollo 15 lunar heat-flow measurement. Moon 4 (3–4), 390–410.

Lucey, P.G., Blewett, D.T., Hawke, B.R., 1998. Mapping the FeO and TiO_2 content of the lunar surface with multispectral imagery. J. Geophys. Res. 103 (E2), 3679–3699. doi:10.1029/97JE03019.

Mezger, P.G., Strassl, H., 1959. The thermal radiation of the Moon at 1420 Mc/s. Planet. Space Sci. 1, 213–226.

Paige, D., Siegler, M., Zhang, J., et al., 2010. Diviner lunar radiometerobservations of cold traps in the Moon's south polar region. Science 330 (6003), 479–482. doi:10.1126/science.1187726.

Pieters, C., Shkuratov, Y., Kaydash, V., et al., 2006. Lunar soil characterization consortium analyses: Pyroxene and maturity estimates derived from Clementine image data. Icarus 184 (1), 83–101. doi:10.1016/j.icarus.2006.04.013.

Price, S.D., Mizuno, D., Murdock, T.L., 2003. Thermal profiles of the eclipsed moon. Adv. Space Res. 31 (11), 2299–2304. doi:10.1016/S0273-1177(03)00531-3.

Shevchenko, V.V., Skobeleva, T.P., Kvaratskhelia, O.I., 2003. A spectropolarimetric maturity index of lunar soil. Sol. Syst. Res. 37 (3), 178–197. doi:10.1023/A:1024002715139.

Vasavada, A., Paige, D., Wood, S., 1999. Near-surface temperatures on Mercury and the Moon and the stability of polar ice deposits. Icarus 141, 179–193.
Vasavada, A.R., Bandfield, J.L., Greenhagen, B.T., et al., 2012. Lunar equatorial surface temperatures and regolith properties from the Diviner Lunar Radiometer Experiment. J. Geophys. Res. Planets 117 (E12). doi:10.1029/2011JE003987.
Wessel, P., Smith, W.H., 1991. Free software helps map and display data. Eos, Trans. Am. Geophys. Union 72 (41), 441–446.
Wesselink, A.F., 1948. Heat conduction and nature of the lunar surface material. Bull. Astron. Inst. Netherlands 390, 351–363.
Zheng, Y., Tsang, K., Chan, K., et al., 2012. First microwave map of the Moon with ChangE-1 data: The role of local time in global imaging. Icarus 219 (1), 194–210. doi:10.1016/j.icarus.2012.02.017.
Zhou, M., Zhou, J., Zhang, X., et al., 2010. Inversion of microwave brightness temperature data for estimating lunar regolith thickness. Int. J. Appl. Electromagnet. Mech. 33 (3–4), 1041–1048. doi:10.3233/JAE-2010-1218.